

Multiplicity, average transverse momentum and azimuthal anisotropy in U+U collisions at $\sqrt{s_{NN}} = 200$ GeV using AMPT model

Md. Rihan Haque¹, Zi-Wei Lin², and Bedangadas Mohanty¹

¹Variable Energy Cyclotron Centre, Kolkata 700064, India and ²Department of Physics, East Carolina University, Greenville, NC 27858-4353, USA

(Dated: October 1, 2018)

Using a multi-phase transport (AMPT) model that includes the implementation of deformed Uranium nuclei, we have studied the centrality dependence of the charged particle multiplicity (N_{ch} , $dN_{ch}/d\eta$), average transverse momentum ($\langle p_T \rangle$), eccentricity ($\langle \varepsilon_2 \rangle$), triangularity ($\langle \varepsilon_3 \rangle$), their fluctuations, elliptic flow (v_2) and triangular flow (v_3) for different configurations of U+U collisions at midrapidity for $\sqrt{s_{NN}} = 200$ GeV. The calculations have been done for both the default and string melting versions of the AMPT model. The results are compared to the corresponding observations from Au+Au collisions. We find that for the U+U collisions the $dN_{ch}/d\eta$ at midrapidity is enhanced by about 15-40% depending on the collision and model configuration chosen, compared to Au+Au collisions. Within the several configurations studied, the tip-to-tip collisions leads to the largest values of N_{ch} , transverse energy (E_T) and $\langle p_T \rangle$. The $\langle \varepsilon_2 \rangle$ and its fluctuation shows a rich centrality dependence, whereas not much variations are observed for $\langle \varepsilon_3 \rangle$ and its fluctuations. The U+U side-on-side collision configuration provides maximum values of $\langle \varepsilon_2 \rangle$ and minimum values of eccentricity fluctuations, whereas for peripheral collisions and mid-central collisions minimum values of $\langle \varepsilon_2 \rangle$ and maximum value of eccentricity fluctuations are observed for body-to-body configuration and the tip-to-tip configuration has minimum value of $\langle \varepsilon_2 \rangle$ and maximum value of eccentricity fluctuations for central collisions. The calculated v_2 closely correlates with the eccentricity in the model. It is smallest for the body-to-body configuration in peripheral and mid-central collisions while it is minimum for tip-to-tip configuration in central collisions. For peripheral collisions the v_2 in U+U can be about 40% larger than in Au+Au whereas for central collisions it can be a factor 2 higher depending on the collision configuration. It is also observed that the $v_3(p_T)$ is higher for tip-to-tip and body-to-body configurations compared to other systems for the collision centrality studied.

PACS numbers: 25.75.Ld

I. INTRODUCTION

In Au+Au collisions at the Relativistic Heavy Ion Collider facility, large values of elliptic flow and large suppression in high transverse momentum hadron production relative to the $p+p$ collisions have been reported [1]. The dominant interpretation of these measurements have indicated that the relevant degrees of freedom in these collisions are quarks and gluons. Deformed nuclei collisions such as U+U will allows us to investigate the initial conditions, hydrodynamic behavior, path length dependence of partonic energy loss [2–4], possible local parity violation [5] and other physics topics beyond what we have learned from Au+Au collisions. The commissioning of the Electron Beam Ion Sources [6] will enable RHIC to collide Uranium ions. U+U collisions are being planned for 2012 with center of mass energy around 200 GeV [7].

In contrast to central Au+Au collisions, because of the prolate shape of Uranium, there are configurations (e.g body-to-body, defined later) in which central U+U collisions are not spherical in the transverse plane, but has an elliptic shape. At RHIC we have observed an increase in v_2/ε_2 with increase in transverse particle density [1]. This corresponds to the dilute regime predictions in kinetic theory [8].

For the hydrodynamic regime, one expects v_2/ε_2 to saturate with increase in transverse particle density [8]. One way to extend the transverse particle density beyond what has been achieved at RHIC is by performing U+U collisions or going to higher beam energies as at LHC. Studies suggest that the maximum transverse particle density attended in U+U collisions could be about 6%-35% higher than Au+Au collisions depending on the colliding configuration [2, 3, 9]. Furthermore, several possible configurations of U+U collisions can occur, depending on the angles of the two incoming Uranium nuclei relative to the reaction plane. This will help in constraining the initial condition models by the measurement of v_2 , v_3 and their fluctuations in U+U and comparing the same to the corresponding results in Au+Au collisions. Galuber-based model simulations suggest an increased value of $\langle \varepsilon_2 \rangle$ (up to 30%) and eccentricity fluctuations in deformed U+U collisions relative to Au+Au collisions [4, 10].

Furthermore it has been shown from the space-time evolution of high energy non-central symmetric heavy ion collisions using relativistic hydrodynamics that the matter expands preferentially in the impact parameter direction and the expanding shells leave a rarefaction behind. As a consequence of early pressure gradient this could at freeze-out lead to three

distinct fireballs being produced. This was referred to as the nutcracker scenario [11]. Subsequently it has been pointed out that such a phenomena is missing for U+U collisions due to the time evolution of the initial transverse energy density profile within a hydrodynamical frame work [12].

The energy loss of partons in a hot and dense colored QCD matter depends not only on the medium density and color factor but also on the path length traversed by the parton. Theories of energy loss for fast partons support a non-linear dependence of parton energy loss on the path-length, but this has not yet been fully tested in experiment, due to the small difference in path lengths for the parton traversing in-plane and out-of-plane for Au+Au collisions. Body-to-body U+U collisions are expected to provide almost twice as much difference between the in-plane and out-of-plane path lengths for the same eccentricity as semi-peripheral Au+Au collisions. This in turn is expected to increase by 100% the absolute value of radiative energy loss and its difference between in-plane and out-of-plane directions [2].

Parity is conserved globally in the strong interaction, but local parity violation is possible because of the topological structure of QCD [13]. It has been proposed that heavy-ion collisions at high energies, provide an unique opportunity to observe local parity violation [14]. The magnetic field required for the parity violating signal exists in non-central heavy-ion collisions and is produced due to the spectators. In central U+U body-to-body collisions, there are no spectators (small or zero magnetic field), while in certain configurations the geometry of the collision zone induces finite v_2 . Background process to local parity violation are expected to be related to v_2 , while the signal is expected to be related to the magnetic field strength [5]. One can then use a comparative study of local parity violation observables for Au+Au and U+U collisions at similar energies to interpretate the measurements [15].

Most of the previous model based study of U+U collisions have made use of Monte Carlo Galuber simulation [4, 10] or it is coupled to a hydrodynamic evolution [2, 3]. Some investigations exists for selecting special orientations of U+U collisions using event generators [9]. In this work, we mainly focus on centrality dependence of $dN_{\text{ch}}/d\eta$, $\langle p_T \rangle$, ε_2 , ε_3 , their fluctuations, v_2 and v_3 for several configurations of U+U collisions. The results are also compared to corresponding observations in Au+Au collisions.

The paper is organized as follows. In the next section we discuss the implementation of U+U collision in the AMPT model [16]. We also discuss the specific configurations of U+U collisions that we study in this paper. Section III presents the results, which includes the N_{ch} , $dN_{\text{ch}}/d\eta$, E_T and $\langle p_T \rangle$. This is fol-

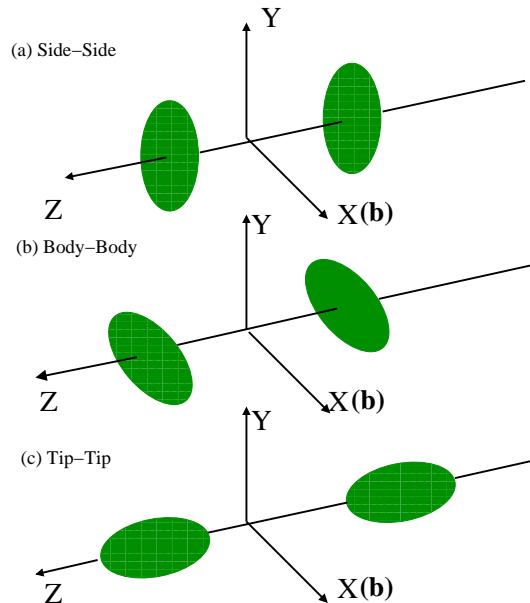


FIG. 1: (Color online) Different configurations of U+U collisions studied in the present work. The Z-axis is the beam direction. X(b) represents that the impact parameter direction is along the X-axis. For more details refer to text and Table I.

lowed by discussion on several geometrical variables like ε_2 , eccentricity fluctuations, ε_3 and its fluctuations. Finally we present results on centrality and transverse momentum dependence of v_2 and v_3 . All results are obtained using both the default and string melting versions of the AMPT model [16] and the U+U results are compared to corresponding results from Au+Au collisions. Finally in section IV we present a summary of our findings.

II. IMPLEMENTING URANIUM COLLISIONS IN AMPT

In the current work, U+U collision is implemented in the AMPT model as follows. The nucleon density distribution is parameterized as a deformed Woods-Saxon profile [17]

$$\rho = \frac{\rho_0}{1 + \exp([r - R']/a)}, \quad (1)$$

$$R' = R [1 + \beta_2 Y_2^0(\theta) + \beta_4 Y_4^0(\theta)], \quad (2)$$

where ρ_0 is the normal nuclear density, R is the radius of the nucleus and a denotes the surface diffuseness parameter. We have used $R = 6.81$ fm and $a = 0.55$ fm for ^{238}U nucleus. The $Y_l^m(\theta)$ denotes the spherical harmonics and θ is the polar angle with the symmetry axis of the nucleus. Deformation parameters are $\beta_2 = 0.28$ [2] and $\beta_4 = 0.093$ [18] for

TABLE I: The details of the angular configuration of U+U collisions used in this study. The subscript p and t denotes the projectile and target respectively. In the simulations, for tip-to-tip configuration the θ is varied as 0 ± 0.07 radian; for body-to-body the θ is varied as $\pi/2 \pm 0.005$ radian and ϕ as 0 ± 0.0025 radian and for side-on-side, the θ and ϕ are varied as $\pi/2 \pm 0.005$ and $\pi/2 \pm 0.17$ radians respectively.

Configuration	θ_p	θ_t	ϕ_p	ϕ_t	Impact parameter
general	$0-\pi$	$0-\pi$	$0-2\pi$	$0-2\pi$	random
tip-to-tip	0	0	$0-2\pi$	$0-2\pi$	minor axis
body-to-body	$\pi/2$	$\pi/2$	0	0	major axis
side-on-side	$\pi/2$	$\pi/2$	$\pi/2$	$\pi/2$	minor axis

Uranium. The presence of β_4 modifies the shape of Uranium compared to that only with β_2 [2, 9]. The radius increases $\sim 6\%$ (3%) at $\theta = 0$ ($\theta = \pi/2$), while it decreases $\sim 3\%$ around $\theta = \pi/4$ [4]. The positions of nucleons are sampled by $4\pi r^2 \sin(\theta) \rho(r) d\theta d\phi$, where the absolute normalization of $\rho(r)$ is irrelevant. Both projectile and target U nuclei are randomly rotated along the polar and azimuthal directions event-by-event with the probability distribution $\sin\Theta$ and uniform distribution for Θ and Φ , respectively. The $\sin\Theta$ weight needs to be implemented to simulate unpolarized nucleus-nucleus collisions.

In this work primarily three types of configuration of U+U collisions are studied and compared to U+U collisions without any specific choice of orientation and Au+Au collisions. These specific configurations will be termed as body-to-body, side-on-side and tip-to-tip in the rest of the paper and are shown in Fig. 1. The details in terms of θ and ϕ angles of the orientation of the nuclei for these configurations studied in this paper are given in Table I.

The AMPT model takes initial conditions from HIJING [19]. However the mini-jet partons are made to undergo scattering before they are allowed to fragment or recombine into hadrons. The string melting version of the AMPT model (labeled here as SM) is based on the idea that for energy densities beyond a critical value of $\sim 1 \text{ GeV}/fm^3$, it is difficult to visualize the coexistence of strings (or hadrons) and partons. Hence the need to melt the strings to partons. This is done by converting the mesons to a quark and anti-quark pair, baryons to three quarks etc. The scattering of the quarks are based on parton cascade ZPC [16]. Once the interactions stop, the partons then hadronizes through the mechanism of parton coalescence. The interactions between the mini-jet partons in default AMPT model and those between partons in the AMPT-SM model could give rise to substantial $\langle v_2 \rangle$. The parton-parton interaction cross section is taken as 10 mb. The results

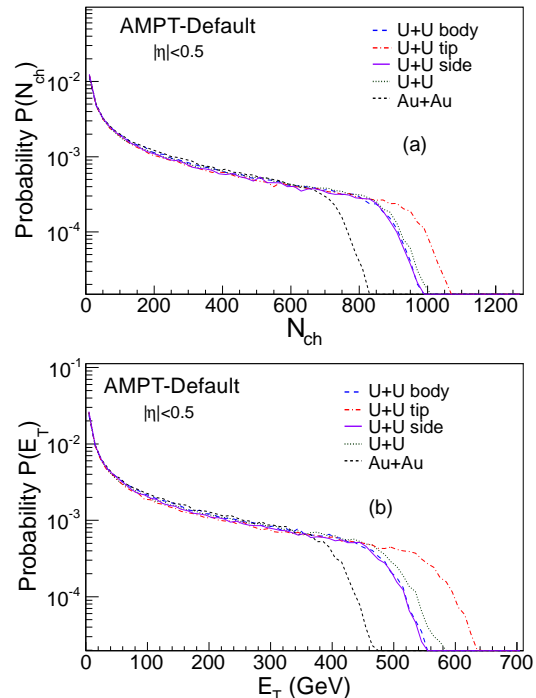


FIG. 2: (Color online) (a) Probability distribution of total charged particle multiplicity (N_{ch}) and (b) charged particle transverse energy (E_T). Both results are at midrapidity ($|\eta| < 0.5$) for minimum bias U+U collisions at $\sqrt{s_{NN}} = 200$ GeV from default AMPT model. The different colored lines corresponds to different configurations of U+U collisions. Also shown for comparison are the results from Au+Au collisions at $\sqrt{s_{NN}} = 200$ GeV from default AMPT model as short dashed lines.

presented below uses both the default and SM version of the AMPT model.

III. RESULTS

A. Multiplicity, transverse energy and average transverse momentum

Figure 2 shows default AMPT model simulated minimum bias charged particle multiplicity (N_{ch}) and charged particle transverse energy (E_T) distributions at midrapidity ($|\eta| < 0.5$) in U+U collisions for different configurations for $\sqrt{s_{NN}} = 200$ GeV. For comparison also shown in Fig. 2 are the results from Au+Au (symmetric nuclei) collisions for the same kinematic conditions. The shapes of the distributions are very similar for different configurations of U+U collisions and those from Au+Au collisions. However the maximum values of N_{ch} and E_T attained for U+U collisions in various configurations is found to be about 15%-35% higher than the corresponding values from Au+Au collisions. The

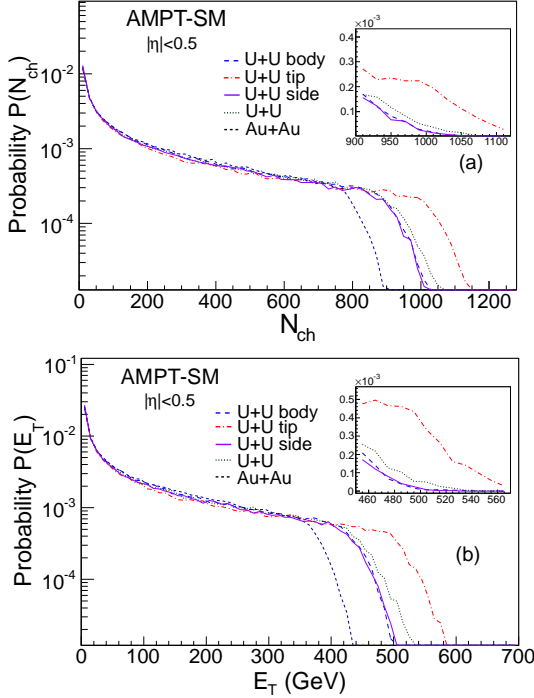


FIG. 3: (Color online) Same as Fig. 2 for AMPT string melting version. The inset shows the distributions for central collisions in an expanded scale.

tip-to-tip configuration in U+U collisions allows to attain the maximum N_{ch} and E_T values among the various cases studied. The rest of the configurations for U+U seems to give similar values.

Figure 3 shows the corresponding results using the string melting version of the AMPT model. The inset of the figure shows the distributions for central collisions in an expanded scale. In general the charged particle multiplicity is about 8% higher compared to the default case. However the transverse energy of charged particles at midrapidity is about 10% lower for string melting case compared to default version of AMPT. The rest of the trends for different configurations for U+U collisions relative to each other and to the Au+Au collisions are similar in the both versions of the model.

Figure 4(a) shows $dN_{ch}/d\eta$ for central collisions (impact parameter $b < 3.6$ fm) vs. η , Fig. 4(b) $(dN_{ch}/d\eta)/(N_{part}/2)$ vs. N_{part} and Fig. 4c charged particle average transverse momentum $\langle p_T \rangle$ vs. N_{part} for different collision configuration of U+U collisions and Au+Au collisions at $\sqrt{s_{NN}} = 200$ from default AMPT model, where N_{part} is the number of participating nucleons. The shape of the $dN_{ch}/d\eta$ are similar for all collision configuration studied and in terms of multiplicity the conclusions are same as seen in Fig. 2(a). The $(dN_{ch}/d\eta)/(N_{part}/2)$ at at midrapidity ($|\eta| < 0.5$) in U+U collisions extends to

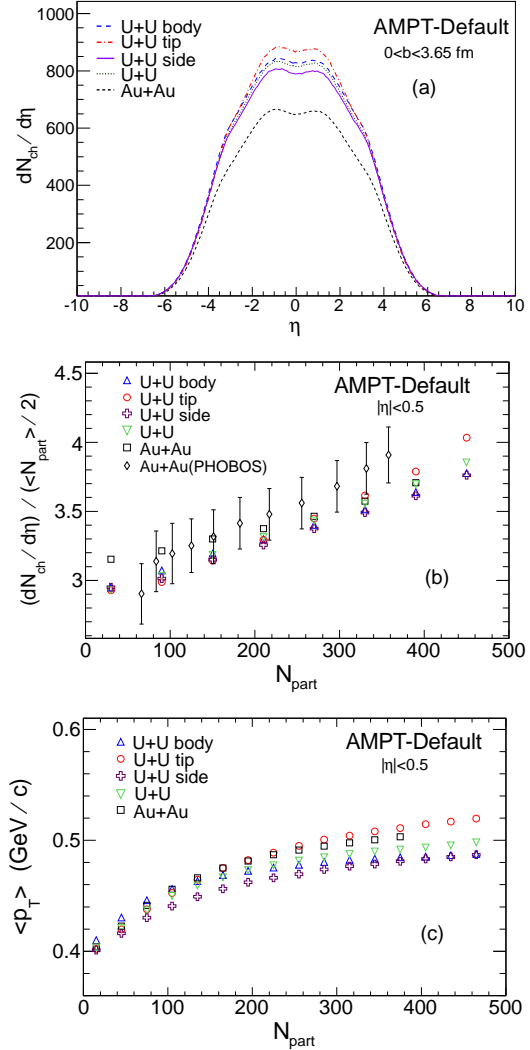


FIG. 4: (Color online) (a) Charged particle pseudorapidity ($dN_{ch}/d\eta$) distribution for central collisions (impact parameter = 3.65 fm) as a function of pseudorapidity (η) for U+U collisions with different configurations of collision and Au+Au collisions at $\sqrt{s_{NN}} = 200$ GeV using default AMPT model. (b) $dN_{ch}/d\eta$ per participating nucleon (N_{part}) pair versus N_{part} at midrapidity ($|\eta| < 0.5$) for above cases. Also shown are the experimental results from Au+Au collisions from PHOBOS experiment at RHIC [20]. (c) Average transverse momentum ($\langle p_T \rangle$) of charged particles as a function of N_{part} at midrapidity ($|\eta| < 0.5$) for above collision configurations.

higher N_{part} values compared to Au+Au collisions. As expected it increases with increase in N_{part} . The charged particle multiplicity in most central collisions studied shows a trend of body-to-body and side-on-side values being similar and lower than the values for tip-to-tip case with $(dN_{ch}/d\eta)/(N_{part}/2)$ values for the general U+U collisions lying in between. The Au+Au collision values for central col-

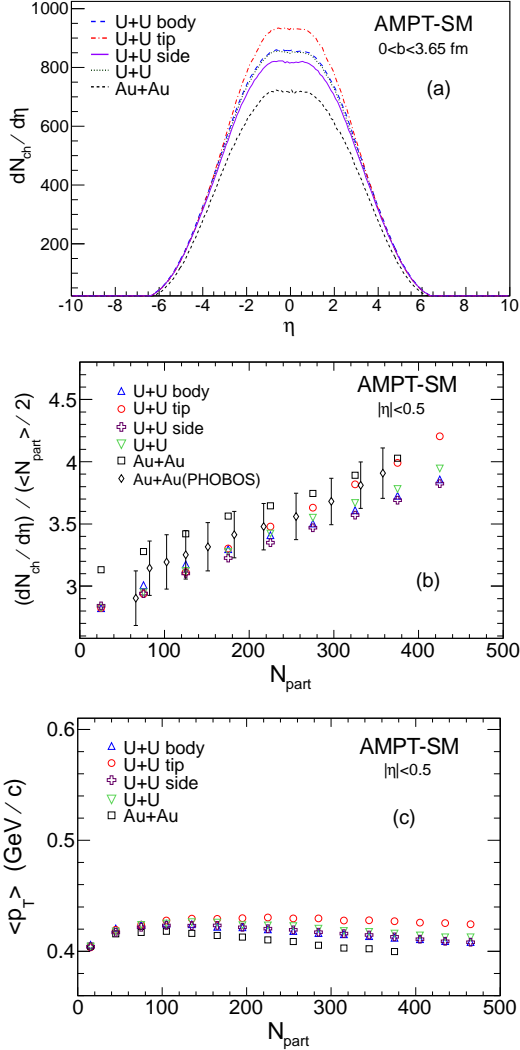


FIG. 5: (Color online) Same as Fig. 4 for AMPT string melting version.

lisions are similar to those from the general U+U configuration case for similar N_{part} . The charged particle $\langle p_T \rangle$ at midrapidity increases with increase in N_{part} . For central collisions the $\langle p_T \rangle$ for tip-to-tip is about 30 MeV higher than the body-to-body case with general U+U configuration $\langle p_T \rangle$ values lying in between. The increase in $\langle p_T \rangle$ at midrapidity ($|\eta| < 0.5$) for U+U tip-to-tip collisions relative to Au+Au collisions is small and is about 10 MeV.

Figure 5 shows the same results as in Fig. 4 using the string melting version of the AMPT model. The conclusions from $dN_{ch}/d\eta$ are similar as for the default case, except that the $dN_{ch}/d\eta$ values are higher in the string melting version. The charged particle $\langle p_T \rangle$ trends with respect to N_{part} is however different. The $\langle p_T \rangle$ values are lower for the string melting version compared to default case and it saturates or

slightly decreases as one goes to central collisions. The saturation of $\langle p_T \rangle$ values for central collisions in the string melting version could be due to additional partonic interactions and the quark coalescence process in the model relative to that for the default case.

B. Geometrical variables

We have followed the notations for the participant eccentricity (ε_2) and triangularity (ε_3) as studied in Ref [21]. The participant eccentricity is defined as:

$$\varepsilon_2 = \frac{\sqrt{\langle r^2 \cos(2\phi_{part}) \rangle^2 + \langle r^2 \sin(2\phi_{part}) \rangle^2}}{\langle r^2 \rangle} \quad (3)$$

where r and ϕ_{part} are the polar coordinate positions of participating nucleons in the AMPT model. Similar to the definition of the eccentricity the participant triangularity, ε_3 is defined as:

$$\varepsilon_3 = \frac{\sqrt{\langle r^2 \cos(3\phi_{part}) \rangle^2 + \langle r^2 \sin(3\phi_{part}) \rangle^2}}{\langle r^2 \rangle} \quad (4)$$

Figure 6 shows the $\langle \varepsilon_2 \rangle$ and $\langle \varepsilon_3 \rangle$ vs. N_{part} for various configurations of U+U collisions at $\sqrt{s_{NN}} = 200$ GeV and Au+Au collisions at $\sqrt{s_{NN}} = 200$ GeV from default AMPT model. For the same N_{part} the U+U collisions without any specific selection of collision configuration have higher $\langle \varepsilon_2 \rangle$ compared to Au+Au collisions. For U+U collisions the tip-to-tip configuration has a lower $\langle \varepsilon_2 \rangle$ compared to no specific selection of collision configuration. The side-on-side configuration have the largest values of $\langle \varepsilon_2 \rangle$ for the systems studied. The $\langle \varepsilon_2 \rangle$ for body-to-body configuration shows a specific trend as a function of N_{part} , it is similar to side-on-side and tip-to-tip in most peripheral collisions, then decreases sharply to values below those from tip-to-tip collisions for mid central collisions which is followed by an increase in values of $\langle \varepsilon_2 \rangle$ with N_{part} to reach the same values as side-on-side for the most central collisions. This clearly reflects the specific geometrical configuration traversed by the two Uranium nuclei in different cases. The $\langle \varepsilon_3 \rangle$ however is found to be similar for all configurations in U+U studied and for Au+Au collisions as a function of N_{part} . Since these are specific to geometrical configurations of the nuclei, we observe no difference in these variable for the string melting version of the model.

Next we study the fluctuation in ε_2 and ε_3 as it has important consequences on understanding of the initial conditions in heavy-ion collisions as well as flow fluctuations. The observables used are the ratio of root mean square (rms) value of ε_2 to $\langle \varepsilon_2 \rangle$, rms of ε_3 to $\langle \varepsilon_3 \rangle$ and those suggested in Ref. [22]: $\langle \varepsilon_n^4 \rangle / \langle \varepsilon_n^2 \rangle^2$

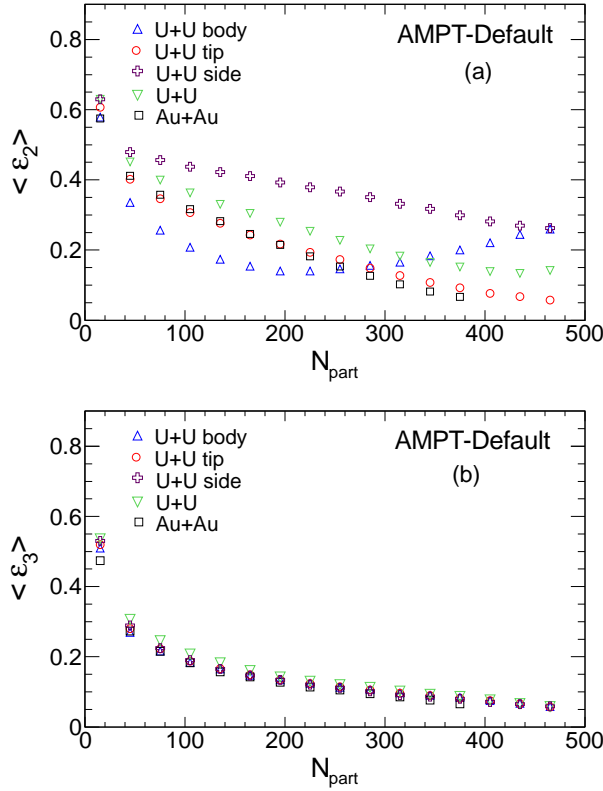


FIG. 6: (Color online) (a) Participant eccentricity ($\langle \varepsilon_2 \rangle$) and (b) triangularity ($\langle \varepsilon_3 \rangle$) as a function of number of participating nucleons (N_{part}) for various configurations of U+U collisions and Au+Au collisions at $\sqrt{s_{\text{NN}}} = 200$ GeV from default AMPT model.

(for $n = 2, 3$ in this work). Figure 7(a) and (b) shows the event-by-event fluctuations in ε_2 and ε_3 as a function of N_{part} for U+U and Au+Au collisions at $\sqrt{s_{\text{NN}}} = 200$ GeV respectively. The fluctuations in ε_2 for U+U collisions with no specific selection on collision configuration closely follows those for Au+Au collisions, however for the most central collisions the fluctuations are slightly smaller for U+U collisions. The fluctuations in ε_2 for tip-to-tip configuration are comparable to those for Au+Au collisions. The fluctuations in ε_2 for side-on-side configuration are the smallest among the configurations studied. On the other hand, those for body-to-body U+U collisions reflects a unique trend with fluctuations in ε_2 being largest in mid-central collisions and then decreasing with increase in centrality to reach the corresponding values of side-on-side for central most collisions. Exactly similar trends are observed using the variable $\langle \varepsilon_n^4 \rangle / \langle \varepsilon_n^2 \rangle^2$ as a function of fraction of collision centrality (Fig. 7 (c) and (d)). In the Figs. 7 (c) and (d) the x-axis value near 0 means most-peripheral and the value near 1 means most-central collisions. The centrality is determined from

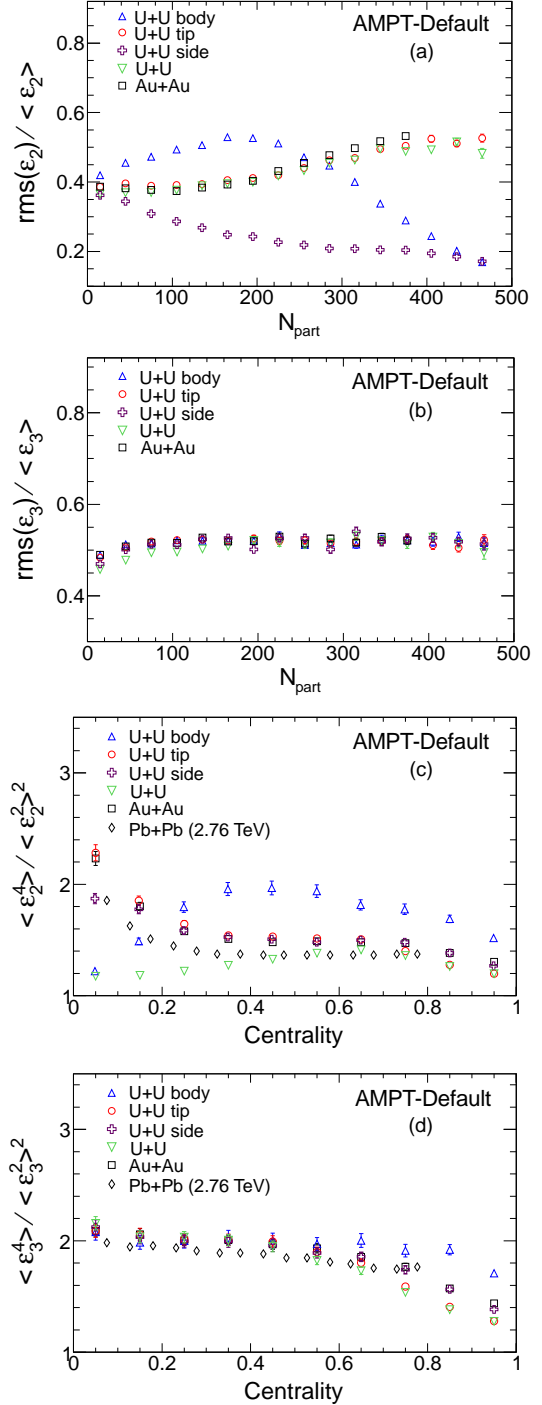


FIG. 7: (Color online) (a) Ratio of root mean square (rms) value of ε_2 to $\langle \varepsilon_2 \rangle$ and (b) rms of ε_3 to $\langle \varepsilon_3 \rangle$ vs. N_{part} for various configurations of U+U collisions and Au+Au collisions at $\sqrt{s_{\text{NN}}} = 200$ GeV using default AMPT model. (c) and (d) $\langle \varepsilon_n^4 \rangle / \langle \varepsilon_n^2 \rangle^2$, with $n = 2, 3$, versus fraction of collision centrality for U+U and Au+Au collisions at $\sqrt{s_{\text{NN}}} = 200$ GeV using the default AMPT model. The Pb+Pb results corresponds to Glauber model simulations from Ref. [22] at $\sqrt{s_{\text{NN}}} = 2.76$ TeV.

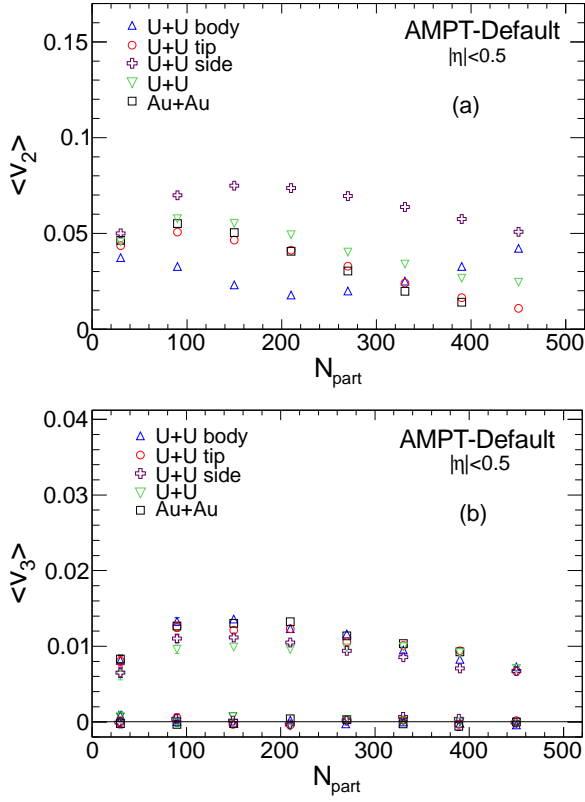


FIG. 8: (Color online) (a) Average elliptic flow ($\langle v_2 \rangle$) and (b) triangular flow ($\langle v_3 \rangle$) versus N_{part} for different collision configuration of U+U and Au+Au collisions at midrapidity for $\sqrt{s_{\text{NN}}} = 200$ GeV from default AMPT model. In (b) the $\langle v_3 \rangle$ values close to zero are those corresponding to $\langle v_3 \rangle$ calculated using ψ_2 .

the impact parameter distribution. The fluctuation in ε_3 are observed to be independent of the collision configuration in U+U and similar to Au+Au collisions, except perhaps for the central most collisions. For comparison results from a Glauber model simulation for Pb+Pb collisions at $\sqrt{s_{\text{NN}}} = 2.76$ TeV from Ref. [22] are also shown. Our study shows that if different U+U configurations can be selected in experimental data, it would lead to interesting variations of flow and flow fluctuations as a function of collision centrality, thereby providing a way to understand initial conditions in heavy-ion collisions at high energies.

C. Elliptic and Triangular flow

The elliptic flow v_2 which is the second Fourier coefficient of particle distribution with respect to ψ_2 is given as

$$v_2 = \langle \cos(2(\phi - \psi_2)) \rangle \quad (5)$$

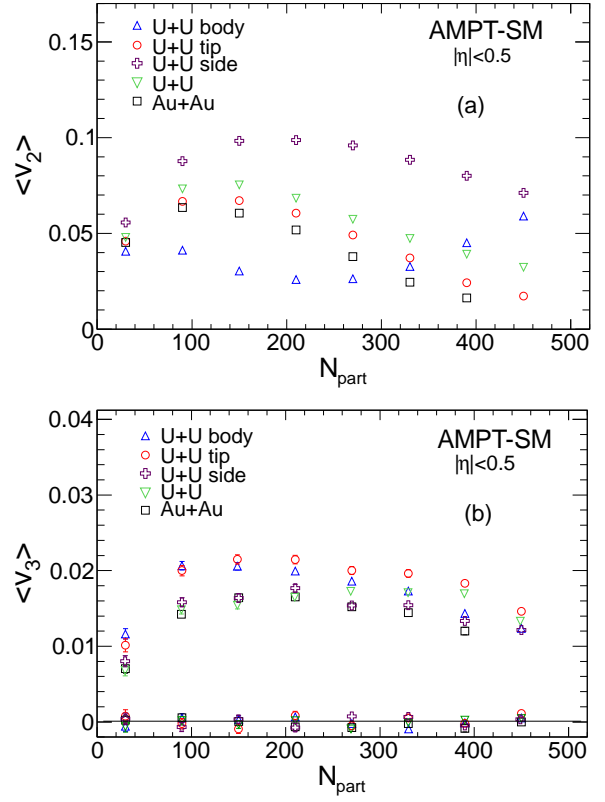


FIG. 9: (Color online) Same as Fig. 8 for AMPT string melting version.

where ψ_2 is the minor axis of the ellipse defined as

$$\psi_2 = \frac{\text{atan2}(\langle r^2 \sin(2\phi_{\text{part}}) \rangle, \langle r^2 \cos(2\phi_{\text{part}}) \rangle) + \pi}{2}. \quad (6)$$

Similar to the definition of the elliptic flow and ψ_2 , the triangular flow, v_3 and ψ_3 are defined as:

$$v_3 = \langle \cos(3(\phi - \psi_3)) \rangle \quad (7)$$

where ψ_3 is the minor axis of participant triangularity given by

$$\psi_3 = \frac{\text{atan2}(\langle r^2 \sin(3\phi_{\text{part}}) \rangle, \langle r^2 \cos(3\phi_{\text{part}}) \rangle) + \pi}{3}. \quad (8)$$

Figure 8(a) and (b) shows the $\langle v_2 \rangle$ and $\langle v_3 \rangle$ as a function of N_{part} at midrapidity ($|\eta| < 0.5$) for different configurations of U+U collisions and Au+Au collisions at $\sqrt{s_{\text{NN}}} = 200$ GeV. The characteristic trend of centrality dependence (smaller values for central collisions and larger values for mid-central collisions) of $\langle v_2 \rangle$ is observed for most of the configurations studied except for U+U body-to-body collisions. In fact the body-to-body collisions shows a minimum $\langle v_2 \rangle$ for mid-central collisions which is consistent with the variation of $\langle \varepsilon_2 \rangle$ with centrality

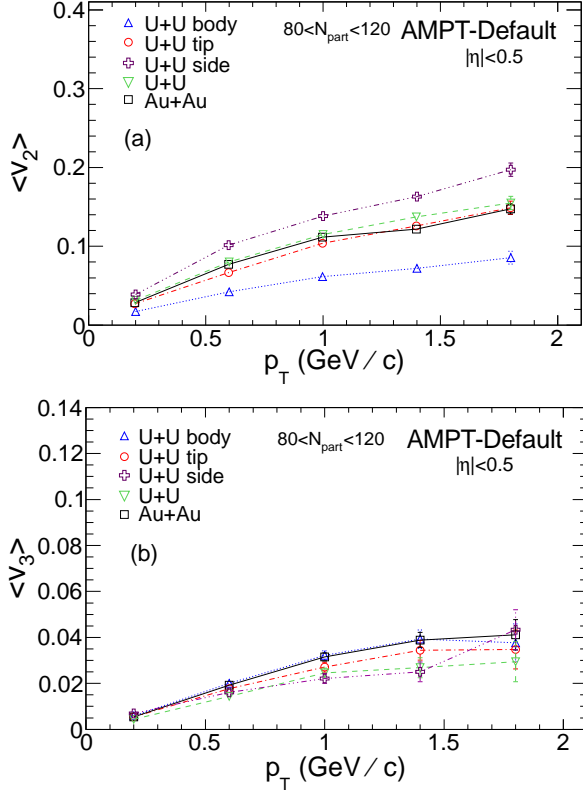


FIG. 10: (Color online) (a) Elliptic flow (v_2) and (b) triangular flow (v_3) as a function of transverse momentum (p_T) at midrapidity for $80 < N_{\text{part}} < 120$ U+U collisions for different configurations and Au+Au collisions at $\sqrt{s_{\text{NN}}} = 200$ GeV from default AMPT model.

as shown in Fig. 7(a). Figure 8(b) shows the corresponding results for v_3 . It is found v_3 is slightly higher for Au+Au collisions compared to U+U collisions without any choice of configuration. For U+U collisions with various configurations the largest v_3 seems to be from body-to-body condition, while those for side-on-side are smaller. Also shown in 8(b) are the $\langle v_3 \rangle$ values (close to zero) when calculated using ψ_2 instead of ψ_3 . The $\langle v_3 \rangle$ value of zero shows that the minor axis of triangularity is found to be uncorrelated with the reaction plane angle for both U+U and Au+Au collisions. The corresponding results for the string melting version are shown in Fig. 9. The conclusions are same as for the default case, except that the magnitude of the $\langle v_2 \rangle$ and $\langle v_3 \rangle$ are typically 40% and 80% higher respectively. Also for $\langle v_3 \rangle$ the tip-to-tip configuration have the largest values while those from Au+Au collisions have smallest values.

Figure 10 and 11 shows the transverse momentum (p_T) dependence of v_2 and v_3 for different collision configuration of U+U and Au+Au collisions at midrapidity ($|\eta| < 0.5$) at $\sqrt{s_{\text{NN}}} = 200$ GeV for

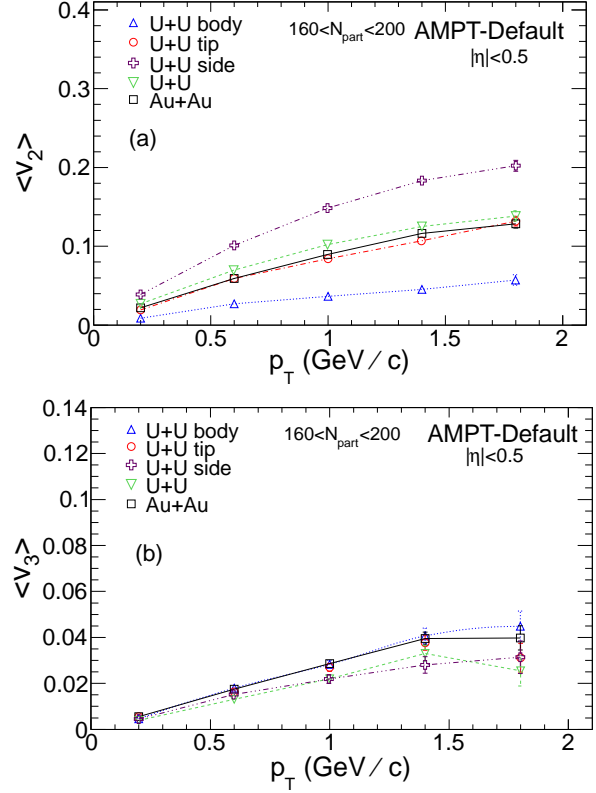


FIG. 11: (Color online) Same as Fig. 10 for $160 < N_{\text{part}} < 200$.

for $80 < N_{\text{part}} < 120$ and for $160 < N_{\text{part}} < 200$ respectively. The $v_2(p_T)$ for U+U collisions without any specific collision configuration, tip-to-tip and Au+Au collisions have similar values for the p_T range studied. The results for $v_2(p_T)$ from body-to-body U+U collisions are smaller and those for side-on-side configuration in U+U collisions are higher compared to Au+Au collisions at similar p_T values. The Fig. 10(b) shows the corresponding results for v_3 . The general trend as observed for p_T integrated v_3 (shown in Fig. 8(b)) is also followed by $v_3(p_T)$. The $v_3(p_T)$ for Au+Au and U+U body-to-body configurations seems to be slightly higher compared to those from U+U tip-to-tip and U+U with no specific configuration selected.

Figure 12 and 13 shows the corresponding results as given in Fig 10 and 11 respectively, for the string melting version of the AMPT model. The general conclusions are similar, except the magnitude of the v_2 and v_3 values are higher for string melting relative to default case. Further one notices the difference in both $v_2(p_T)$ and $v_3(p_T)$ for various collision configuration seems to have increased for string melting case compared to default case. For the several configurations studied the $v_3(p_T)$ in default AMPT model for U+U collisions are mostly below the correspond-

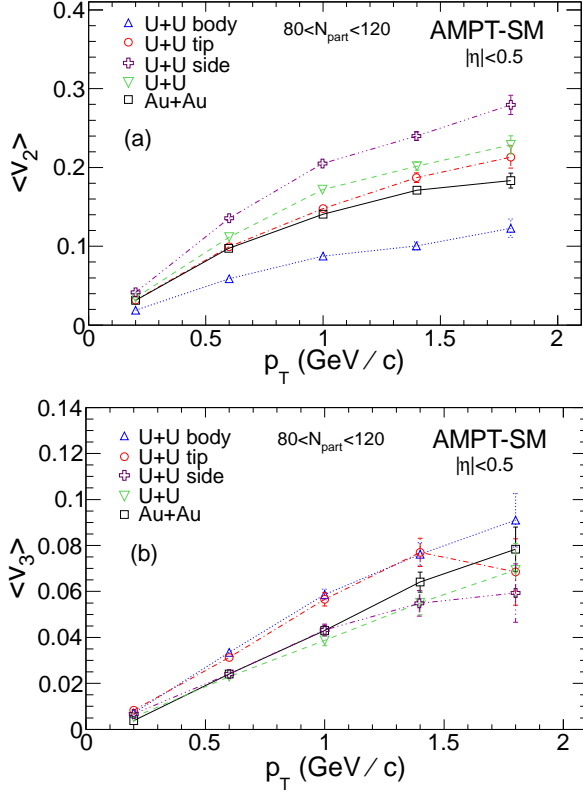


FIG. 12: (Color online) Same as Fig. 10 for AMPT string melting version.

ing values from Au+Au collisions, while for string melting case the U+U collision $v_3(p_T)$ are mostly higher than the corresponding values from Au+Au collisions.

IV. SUMMARY

In this study we have implemented the possibility of studying high energy collisions with deformed Uranium nuclei within the framework of AMPT model. Experimental U+U collisions at around $\sqrt{s_{NN}} = 200$ GeV is planned for the year 2012 at the RHIC facility. The Uranium nuclei is implemented by using a deformed Woods-Saxon profile and the projectile and target Uranium nuclei are randomly rotated along the polar and azimuthal directions event-by-event with the probability distribution $\sin\Theta$ and uniform distribution for Θ and Φ , respectively. In the current work we have studied three specific configurations of U+U collisions for $\sqrt{s_{NN}} = 200$ GeV, based on the choice of the polar, azimuthal angles of the two nuclei and the impact parameter direction. The results from these collisions have been compared to U+U collisions with no specific choice of orientation and Au+Au colli-

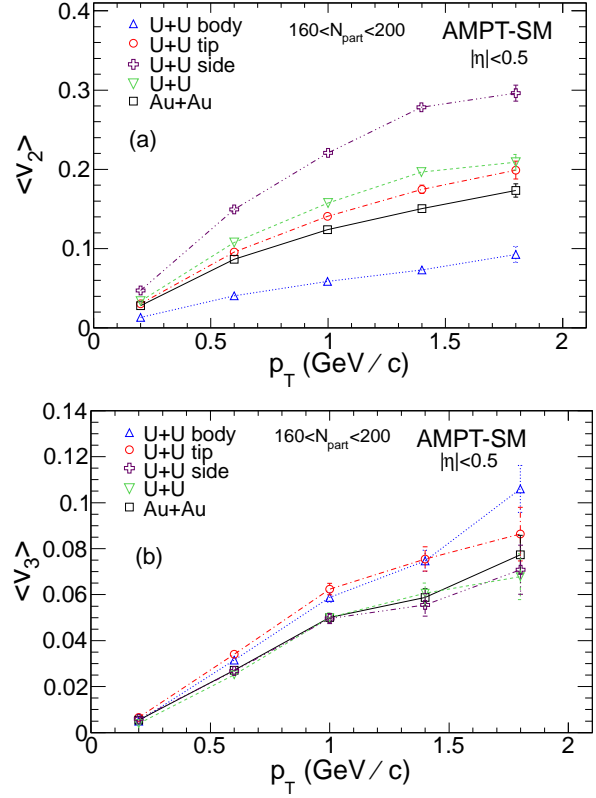


FIG. 13: (Color online) Same as Fig. 12 for $160 < N_{part} < 200$.

sions at the same beam energy. For most of the observables studied we present the results for both default and string melting configurations of the AMPT model.

The charged particle multiplicity and charged particle transverse energy is found to be about 15%–35% higher for the different U+U configurations relative to Au+Au collisions. For string melting version the multiplicities are higher by about 8% for U+U collisions compared to default model, whereas for the transverse energy they are lower by about 10% compared to default. The average transverse momentum for charged particles increases with number of participating nucleons for the default case, whereas they saturate for central collisions in case of the string melting version. This is perhaps due to additional partonic interactions and the quark coalescence process in the string melting model relative to the default case. Within the different configurations studied, the multiplicity, transverse energy and average transverse momentum at midrapidity are largest for the tip-to-tip configuration. This observation may be used in future to select events of particular configuration for U+U collisions.

The average eccentricity and fluctuations in eccentricity shows a rich dependence on collision central-

ity. The side-on-side configuration possesses the maximum eccentricity and minimum eccentricity fluctuations as a function of collision centrality among the configurations studied. On the contrary, the body-to-body configuration has the minimum eccentricity and maximum eccentricity fluctuations for peripheral and mid-central collisions. The tip-to-tip configuration has minimum eccentricity and maximum eccentricity fluctuations for central collisions. We did not observe large variation in triangularity and its fluctuations for different configurations of U+U collisions studied or between U+U collisions and Au+Au collisions.

The variation of eccentricity and its fluctuation gets reflected in dependence of v_2 and v_3 as a function of collision centrality. In both the default and string melting versions of the model, the side-on-side configuration has maximum v_2 compared to all other configurations and Au+Au collisions studied for all collision centrality. The v_2 is smallest for the body-to-body configuration in peripheral and mid-central collisions while it is minimum for tip-to-tip configuration in central collisions. For peripheral collisions the v_2 in U+U can be about 40% larger than in Au+Au whereas for central collisions it can be a factor 2 higher depending on the collision configuration. These features in v_2 closely follow the

features in the ε_2 . The v_3 does not show much dependence on U+U configuration for AMPT calculations in default version, however in string melting version, it seems the body-to-body and tip-to-tip configurations have higher v_3 values as a function of collision centrality compared to other cases studied. The p_T dependence of v_2 is presented for $80 < N_{\text{part}} < 120$ and $160 < N_{\text{part}} < 200$. We observe a U+U side-on-side configuration has largest v_2 while U+U body-to-body configuration has the smallest v_2 . For the other configurations, tip-to-tip, U+U and Au+Au the values are similar. A more clearer p_T dependence of v_3 is observed in string melting case compared to default case. In the string melting case, the v_3 of tip-to-tip and body-to-body are similar and higher than U+U, U+U side-on-side and Au+Au collisions.

The future scope of our study includes studying the effect of jet-quenching and jet-medium interactions via dihadron correlations for different configurations of U+U collisions. Furthermore we plan to use the AMPT model to study the most effective way to select various configuration in U+U collisions in an experiment.

Acknowledgments

This work is supported by the DAE-BRNS project grant No. 2010/21/15-BRNS/2026.

-
- [1] I. Arsene et al., [BRAHMS Collaboration], Nucl. Phys. A **757**, 1 (2005); B.B. Back et al., [PHOBOS Collaboration], Nucl. Phys. A **757**, 28 (2005); J. Adams et al., [STAR Collaboration], Nucl. Phys. A **757**, 102 (2005); K. Adcox et al., [PHENIX Collaboration], Nucl. Phys. A **757**, 184 (2005).
 - [2] U. Heniz and A. Kuhlman, Phys. Rev. Lett. **94**, 132301 (2005); A. Kuhlman and U. Heniz, Phys. Rev. C **72**, 037901 (2005).
 - [3] T. Hirano, P. Huovinen and Y. Nara, Phys. Rev. C **83**, 021902(R) (2011).
 - [4] H. Masui, B. Mohanty and N. Xu, Phys. Lett. B **679**, 440 (2009).
 - [5] S. A. Voloshin, Phys. Rev. Lett. **105**, 172301 (2010).
 - [6] A. Pikin et al., JINST **5**, C09003 (2010).
 - [7] <http://www.bnl.gov/npp/docs/pac0611/Overall%20recommendations%20final.pdf> . BNL program advisory committee recommendations, June 6-8, 2011 (<http://www.bnl.gov/npp/pac.asp>).
 - [8] H. Heiselberg and A. M. Levy, Phys. Rev. C **59**, 2716 (1999).
 - [9] C. Nepali, G. Fai and D. Keane, Phys. Rev. C **76**, 051902(R) (2007); Phys. Rev. C **73**, 034911 (2006).
 - [10] P. Filip, R. Lednicky, H. Masui and N. Xu, Phys. Rev. C **80**, 054903 (2009).
 - [11] D. Teaney and E. V. Shuryak, Phys. Rev. Lett. **83**, 4951 (1999).
 - [12] P. F. Kolb, J. Sollfrank and U. W. Heinz, Phys. Rev. C **62**, 054909 (2000).
 - [13] D. Kharzeev, R. D. Pisarski and M. H. G. Tytgat, Phys. Rev. Lett. **81**, 512 (1998).
 - [14] L. E. Finch, A. Chikanian, R. S. Longacre, J. Sandweiss and J. H. Thomas, Phys. Rev. C **65**, 014908 (2002); S. A. Voloshin, Phys. Rev. C **62**, 044901 (2000).
 - [15] B. I. Abelev et al. [STAR Collaboration], Phys. Rev. Lett. **103**, 251601 (2009).
 - [16] Z. W. Lin and C. M. Ko, Phys. Rev. C **65**, 034904 (2002); Z. W. Lin et al., Phys. Rev. C **72**, 064901 (2005).
 - [17] K. Hagino, N. W. Lwin and M. Yamagami, Phys. Rev. C **74**, 017310 (2006).
 - [18] P. Moller, J. R. Nix, W. D. Myers and W. J. Swiatecki, Atom. Data Nucl. Data Tabl. **59**, 185 (1995).
 - [19] X. N. Wang and M. Gyulassy, Phys. Rev. D **44**, 3501 (1991).
 - [20] B. Alver et al. [PHOBOS Collaboration], Phys. Rev. C **83**, 024913 (2011).
 - [21] B. Alver, G. Roland, Phys. Rev. C **81**, 054905 (2010).
 - [22] R. S. Bhalerao, M. Luzum, J. -Y. Ollitrault, Phys. Rev. C **84**, 054901 (2011).